Neurosci. Bull.
https://doi.org/10.1007/s12264-023-01047-4

www.neurosci.cn
www.springer.com/12264

ORIGINAL ARTICLE

# Lipocalin 2 in the Paraventricular Thalamic Nucleus Contributes to DSS-Induced Depressive-Like Behaviors

**Yeru Chen[1] · Du Zheng[1] · Hongwei Wang[1] · Shuxia Zhang[1] · Youfa Zhou[1] · Xinlong Ke[1] · Gang Chen[1]**

Received: 21 September 2022 / Accepted: 23 January 2023


**Abstract** The incidence rate of anxiety and depression is significantly higher in patients with inflammatory bowel diseases (IBD) than in the general population. The mechanisms underlying dextran sulfate sodium (DSS)-induced depressive-like behaviors are still unclear. We clarified that IBD mice induced by repeated administration of DSS presented depressive-like behaviors. The paraventricular thalamic nucleus (PVT) was regarded as the activated brain region by the number of c-fos-labeled neurons. RNA-sequencing analysis showed that lipocalin 2 (Lcn2) was upregulated in the PVT of mice with DSS-induced depressive behaviors. Upregulating Lcn2 from neuronal activity induced dendritic spine loss and the secreted protein induced chemokine expression and subsequently contributed to microglial activation leading to blood-brain barrier permeability. Moreover, Lcn2 silencing in the PVT alleviated the DSS-induced depressive-like behaviors. The present study demonstrated that elevated Lcn2 in the PVT is a critical factor for DSS-induced depressive behaviors.

**Keywords** Inflammatory bowel disease · Depression · Lcn2 · Blood-brain barrier

## Introduction

Inflammatory bowel disease (IBD), which comprises ulcerative colitis and Crohn's disease, is a chronic inflammatory disorder of the gastrointestinal tract. Evidence has shown that the prevalence of psychiatric comorbidities such as anxiety and depression is significantly higher in patients with IBD than in healthy persons [1]. The mental disorder negatively affects the quality of life and the severity of the inflammatory condition. Depressive symptoms are intimately related to colon inflammatory activity, which is regarded as a strong predictor of disease deterioration [2]. The interaction between IBD and depressive symptoms may be explained by T cell activation [3], tryptophan catabolite pathways [4], and gut dysbiosis [5]. Some research focused on the blood-brain barrier (BBB) integrity underlying depressive symptoms. Impaired BBB integrity has been reported in TNBS (2,4,6-trinitrobenzene sulfonic acid)-induced colitis in Sprague–Dawley rats [6]. However, uncertainties remain about the crucial issues in IBD-induced symptoms of depression.

Several researchers identified the critical role of the hippocampus in linking IBD-induced depression with increased levels of pro-inflammatory cytokines and a reduction in neurogenesis. Depending on the exposure time of dextran sulfate sodium (DSS, a classical reagent for the IBD animal model), inflammatory-related markers show region-specific expression, indicating that different regions need to be investigated to understand the precise mechanisms underlying DSS-induced depression [7]. In the current study, we found that the paraventricular thalamic nucleus (PVT) was activated, based on a large number of c-fos-labeled neurons. Recent studies have described PVT as a crossroads that plays a role in the regulation of negative emotional behavior [8, 9]. The

**Supplementary Information** The online version contains supplementary material available at https://doi.org/10.1007/s12264-023-01047-4.

✉ Gang Chen
chengang120@zju.edu.cn

[1] Department of Anesthesiology, Sir Run Run Shaw Hospital, School of Medicine, Zhejiang University, Hangzhou 310016, China

Published online: 15 March 2023

potential role of PVT in DSS-induced depressive disorders needs to be investigated further.

Lipocalin 2 (Lcn2), also known as neutrophil gelatinase-associated lipocalin, has a variety of biological effects including cell migration, apoptosis, and amplification of the inflammatory response [10]. Lcn2 is regulated in the central nervous system in response to acute and chronic inflammation with the mediation of the morphological changes in reactive glial cells, promoting the activation of microglia and astrocytes [10, 11]. In our work, Lcn2 in the PVT was required for DSS-induced depressive behaviors. Moreover, Lcn2 at a high level in the PVT was the risk factor for microglial activation, which plays an important role in CNS health. We demonstrated that Lcn2 regulated the dendritic spines and microglial activation in the PVT after DSS treatment, providing a novel therapeutic target in DSS-induced depressive-like behaviors.

## Materials and Methods

### Animals

Zhejiang University Animal Experimentation Committee approved the protocol (ZJU20220307), and all experiments were conducted based on its ethical guidelines and in compliance with the National Institutes of Health Guide for the Care and Use of Laboratory Animals. Six-week-old mice were obtained from the Zhejiang Academy of Medical Sciences. A standard animal care facility provided food and water for a month, as well as a 12/12-h light/dark cycle and a constant temperature of 22°C for the duration of the experiment. Our goal was to minimize pain and discomfort for the animals, and we used the smallest number of animals possible.

### Animal Treatment

To induce colitis in mice, male wild-type C57BL/6 mice between 6 and 8 weeks of age were given 2.5% DSS in the drinking water *ad libitum* for 5 days. Then the 2.5 % DSS was replaced by drinking water for 2 days. This procedure is repeated for one more cycle. Mice given regular drinking water throughout the treatment period were used as controls.

### Open Field Test

White plastic boxes were used as open field chambers (dimensions: 45 cm × 45 cm × 45 cm). Mice were individually placed in the center of the chamber and allowed to freely explore for 15 min. The locomotor and exploratory behaviors were recorded using ANY-maze software (Stoelting, Wood Dale, IL, USA). The overall distance traveled was used to evaluate locomotor activity.

### Forced Swimming Test

The protocol of the forced swimming test followed the previous studies [12, 13]. The mice were placed in a glass chamber (35 cm high, 30 cm in diameter) filled with warm water, The water temperature was 22–24 ℃ with a depth of 20 cm. Water depth was set to prevent animals from touching the bottom with their tails or hind limbs. Animal behaviors were videotaped from the side. The mice were allowed to freely swim for 6 min, and the immobile time during the last 4-min test was counted by an observer blinded to animal treatment. Immobile time was defined as the time when animals remained floating or motionless with only movements necessary for keeping balance in the water.

### Tail Suspension Test

The tail suspension test was as described in previous studies [13, 14]. One-third of the mouse's tail was fixed and hung on a support, with its head 20 cm away from the table. Animal behaviors were videotaped from the side. The mice were suspended for 6 min, and the immobile time during the last 4-min test was counted by an observer blinded to animal treatment. Animals were considered to be immobile when they exhibited no body movement and hung passively.

### Sucrose Preference Test

The mice were singly housed and habituated with two bottles of water for 2 days, followed by two bottles of 2% sucrose for 2 days. The mice were water-deprived for 24 h and then exposed to one bottle of 2% sucrose and one bottle of water for 2 h in the dark phase. Bottle positions were switched after 1 h (for a 2-h test). The total consumption of each fluid was measured and sucrose preference was defined as the average sucrose consumption ratio during the first and second hours. The sucrose consumption ratio was calculated by dividing the total consumption of sucrose by the total consumption of both water and sucrose.

### Golgi-cox Staining

We used Golgi-Cox staining to observe the morphology of neuronal dendrites and dendritic spines in the brains of mice. The Hito Golgi-Cox OptimStain PreKit (Hitobiotec Corp. Kingsport, TN, USA) was applied according to previous studies [15]. Each intact brain was rinsed with double-distilled water and impregnated with 5 times volumes of Solutions A and B in the assay kit. The impregnation solution was replaced the following day and the brain was

stored at room temperature away from light for 14 days. The brains were then transferred to 5 times Solution C for further storage at 4°C for 72 h in the dark. The brains were slowly immersed in cooled isopentane and brain sections (120 μm thick) were cut on a cryostat at −19°C. After drying naturally at room temperature for 3 days, the sections were processed as per the manufacturer's instructions. The dendrites within the PVT were imaged using the 20× and 60× objectives of an Olympus BX61 microscope. Dendritic spines were detected along PVT dendrites starting from their point of origin on the primary dendrite, and counting was performed by an experimenter blinded to the group of each sample.

### Immunostaining

Serial cryostat sections, 25 μm thick, were collected according to the method described in previous studies [15, 16]. The sections were incubated with 5% donkey serum and 0.3% Triton X-100 for 1 h at room temperature, then with antibody diluent containing goat antibodies against c-fos (1:1000; Cell Signaling Technology, #2250), Iba-1 (1:200; Abcam, ab178846), Lcn2 (1:200; Abclonal, A2092), ZO-1 (1:200; Abcam, ab190085), Neun (1:200; Abcam, ab104224), GFAP (1:400, Cell Signaling Technology, #3670) Iba1 (1:100; Abcam, ab5076), and 24p3R (1:100; Sigma, SAB3500306) overnight at 4°C. Then the sections were rinsed with PBS (3×10 min) followed by incubation with Alexa Fluor 488 goat anti-mouse antibody, Alexa Fluor 488 goat anti-rabbit antibody, FITC donkey anti-goat IgG (H+L), donkey anti-goat IgG (H+L), and Cross-Adsorbed Secondary Antibody, Alexa Fluor 594 for 1 h at room temperature. For extravascular IgG immunostaining, the sections were incubated with donkey serum and Triton X-100 for 1 h at room temperature. Slides were washed in PBS and incubated with goat anti-mouse IgG Cross-Adsorbed Secondary Antibody, Alexa Fluor 594 (Invitrogen, A-11005, 1:200) for 1 h at room temperature. Fluorescent images were acquired with a Nikon A1 confocal microscope. Images were captured with the assistance of Image-Pro Plus 5.0 software, and all the parameters used were kept consistent during capture.

### Next-Generation Sequencing

For the RNA-Seq analysis, the PVT tissues were obtained from IBD mice and Ctrl mice (3 mice/group). The protocol of RNA sequencing includes RNA extraction, size selection, database building, and sequencing, according to previous studies [17]. Total RNA from different groups was extracted using RNAiso Plus Reagent (TaKaRa, Japan), and purified using an RNeasy Mini Kit (Qiagen) based on the manufacturer's protocol. After measuring the RNA concentration and integrity, the total RNA was treated with DNase I, and eukaryotic mRNA was enriched with magnetic beads with oligo (DT). Then the interruption reagent was added to break the mRNA into short fragments, and the interrupted mRNA was used as a template to synthesize a strand of cDNA with random hexamers, and then a buffer, dNTPs, and DNA polymerase I were added to synthesize the second strand of cDNA. After purification and recovery by the kit, the obtained fragments were amplified and enriched by PCR after size selection. The constructed library was sequenced by the Illumina sequencing platform after passing the quality inspection of the Agilent 2100 Bioanalyzer and ABI steponeplus real-time PCR system.

Raw data obtained by the sequencing platform were filtered through data quality control to obtain high-quality clean reads. We further located the reads of the comparison genome to the gene exon region through Htseq and then counted the number of reads on each gene comparison to estimate the gene expression level.

The differentially-expressed genes (DEGs) obtained from the RNA-seq-based expression profiling were analyzed by DEGseq and DEGseq2 online tools. FPKM (fragments per kilobase of exon per million mapped fragments) is the most common method to estimate the gene expression level considering the effects of sequencing depth and gene length on read counts. Genes specifically upregulated or downregulated were identified by selecting those that had at least a $|\log2FC| > 1$ and a false discovery rate $FDR < 0.05$ in one condition compared with all of the other three.

### Viral Packaging and Stereotactic Injection

The CMV-Lcn2 shRNA adeno-associated virus was constructed and packaged by Vigene Biosciences (Shangdong, China). For Lcn2 shRNA viral packaging, the shRNA sequence of mouse Lcn2 (5′- GCTACTGGATCAGAACAT TTGTTCAAGAGACAAATGTTCTGATCCAGTAGCTTT TTT-3′) was synthesized and cloned into the pAV-U6-GFP plasmid to produce pAV-U6-eGFP-Lcn2 shRNA. Scrambled adeno-associated viruses were regarded as the control virus. Viral particles were purified by iodixanol step-gradient ultracentrifugation. The genomic titer was $9.07 \times 10^{13}$ TU/mL as determined by quantitative PCR.

For viral injection, mice were anesthetized with ketamine (100 mg/kg) and xylazine (8 mg/kg) by intraperitoneal injection and placed in a stereotactic frame. Purified and concentrated adenovirus was injected bilaterally into the paraventricular thalamic nucleus (100 nL, coordinates from bregma, − 1.58 mm anterior/posterior, 0 mm medial/lateral, − 2.75 mm dorsal/ventral) through glass micropipettes at a slow rate (10 nL/min). In the animal experiments, the mice received a virus injection (100 nL) two weeks after DSS treatment. The behavioral tests of all mice were carried out after the DSS treatment. The injection sites were examined at the end of all

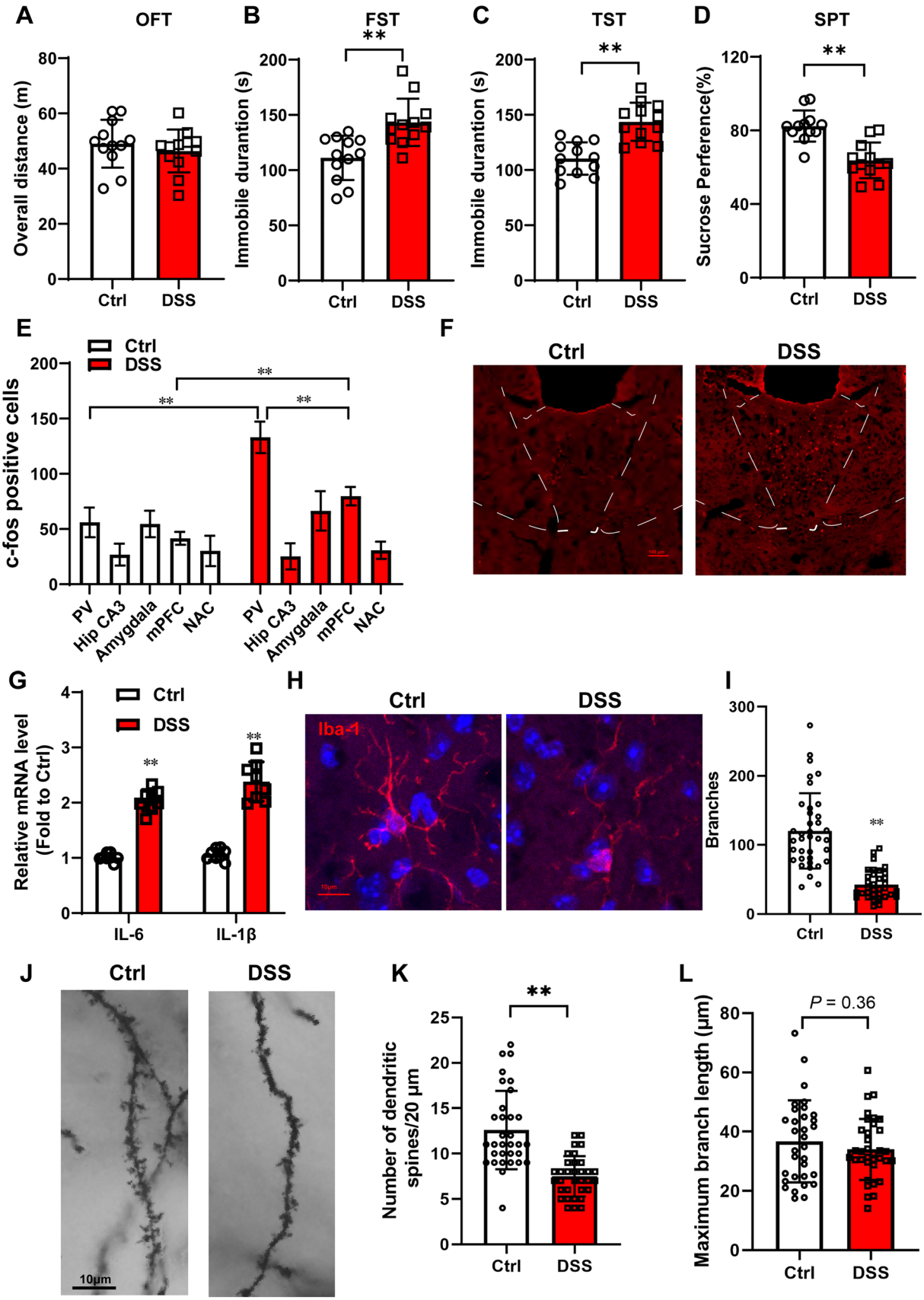
A
OFT
Overall distance (m)
Ctrl
DSS
B
FST
Immobile durantion (s)
**
C
TST
Immobile durantion (s)
**
D
SPT
Sucrose Perference(%)
**
E
Ctrl
DSS
c-fos positive cells
**
PV
Hip CA3
Amygdala
mPFC
NAC
F
Ctrl
DSS
G
Relative mRNA level (Fold to Ctrl)
IL-6
IL-1β
H
Ctrl
DSS
Iba-1
I
Branches
J
Ctrl
DSS
10μm
K
Number of dendritic spines/20 μm
L
P = 0.36
Maximum branch length (μm)

◂**Fig. 1** The paraventricular thalamic nucleus is critical for DSS-induced depressive disorder. Wild-type C57BL/6 mice between 6 and 8 weeks old were given 2.5% DSS in the drinking water *ad libitum* for 2 cycles lasting 2 weeks. **A** Open field ($n=12$), **B** forced swimming ($n=12$), **C** the tail suspension test ($n=12$), and **D** the sucrose preference test ($n=12$) are shown at the end of DSS administration; **E** Analysis of c-fos labeled neuron numbers ($n=3$); **F** Representative images of the expression of c-fos in the paraventricular thalamic nucleus of DSS mice and normal mice. Scale bar 100 μm. **G** The mRNA levels of IL-6 and IL-1β in the PVT of DSS mice and normal mice ($n=8$). **H** Representative images of the expression of Iba-1 in the paraventricular thalamic nucleus of DSS mice and normal mice by immunostaining. **I, L** Analysis of microglial morphology ($n=5$ mice/group). More than 30 images were analyzed for each group. **J** Representative images of Golgi staining in the paraventricular thalamic nucleus of DSS mice and normal mice. **K** Analysis of the numbers of dendritic spines at the unit distance of 20 μm ($n=5$ mice/group). More than 30 images were counted for each group. The data are presented as the mean ± SD. The *t*-test was used for (**A**, **B**, **C**, **D**, **I**, **K**, and **L**) and two-way ANOVA was used for (**E** and **G**) $^{*}P<0.05$. $^{**}P<0.01$.

the behavioral tests and only data from animals with correct injections were collected. Sections through the dentate gyrus were directly examined under a fluorescence microscope.

### Cell Culture and Treatment

SH-SY5Y cells purchased from the China Center for Type Culture Collection were cultured in MEM/F12 (1:1) containing 10% heat-inactivated fetal bovine serum, and 1 mmol/L sodium pyruvate (all from Gibco, Grand Island, NY, USA) at 37 °C with 5% $CO_2$ in a humidified incubator. SH-SY5Y cells were incubated with recombinant Lcn2 protein (Abcam, ab243270) (1 or 10 μg/mL) for 6, 12, or 24 h, and total RNA was isolated for real-time RT-PCR. The mRNA levels of chemokines (CCL2 and CX3CL1) and cytokines (IL-1β and IL-6) were determined. The nucleotide sequences of the primers used in RT-PCR were: CCL2: F, 5'-TCAGCCAGATGCAGTTAACG-3'; R, 5'-GATCCTCTTGTAGCTCTCCAGC-3'; CX3CL1: F, 5'-ACGAAATGCGAAATCATGTGC-3'; R, 5'-CTGTGTCGTCTCCAGGACAA-3'; IL-1β: F, 5'-AAGTTGACGGACCCCAAAAGAT-3'; R, 5'-TGTTGATGTGCTGCTGCGA-3'; IL-6: F, 5'-AGTTGCCTTCTTGGGACTGA-3'; R, 5'-TCCACGATTTCCCAGAGAAC-3'.

### Determination of Evans Blue Dye Extravasation

To evaluate the BBB integrity, Evans blue dye was used as a marker of albumin extravasation as previously described. Briefly, Evans blue dye (2% in saline, 4mL/kg) was injected *via* the tail vein at the end of the induction of the IBD animal model with DSS and allowed to remain in circulation for 1 h. At the end of the experiments, the mice were anesthetized with ketamine (60 mg/kg)and xylazine (5 mg/kg) intraperitoneally and the mice were perfused transcardially with PBS. After the brain was imaged, the PVT was harvested from all mice. The EB-albumin extravasation was then measured in brain tissue homogenates (2.5mL PBS followed by the addition of 2.5mL of 60% trichloroacetic acid, to precipitate the protein). Samples were cooled and then centrifuged for 30 min at 1000 g. The supernatant was measured at 610 nm for absorbance of Evans blue dye using a spectrophotometer against a standard curve. EB was expressed as ng/mg of brain tissue.

### Statistical Analysis

All data were collected and analyzed blindly. Data are presented as the mean ± SEM. Single comparisons were determined by a two-tailed Student's *t*-test. Two-way ANOVA with Tukey's multiple comparisons test was applied for multiple comparisons. Sample sizes were based on our previous study and prior literature to achieve reliable measurements. Statistical analyses were applied using GraphPad Prism 8.0 (GraphPad Software, San Diego, CA, USA). $P<0.05$ was considered statistically significant.

## Results

### The Paraventricular Thalamic Nucleus is Critical for the DSS-Induced Depressive Disorder

Repeated administration of DSS in drinking water is regarded as inducing a well-characterized mouse model of IBD. To measure the depressive-like behavior in DSS mice, a forced swimming test, tail suspension test, and sucrose preference test was used at the end of the DSS treatment. The overall distance did not differ between the Ctrl mice and the DSS mice in the open field test, suggesting that DSS does not impair motor function (Fig. 1A, $P=0.4400$). The duration of immobility in DSS-treated mice was significantly prolonged compared with the Ctrl mice in the forced swimming test (Fig. 1B, $P=0.001$) and tail suspension test (Fig. 1C, $P<0.001$). The sucrose preference was remarkably decreased in DSS mice compared with Ctrl mice (Fig. 1D, $P<0.001$). These data indicated that DSS induced depressive-like behavior.

The hippocampus affects DSS-induced depressive-like behavior, with increased levels of pro-inflammatory cytokines and a reduction in hippocampal neurogenesis [18]. To further identify strongly interactive brain regions, we measured the expression of c-fos, a marker of neural activity, in several brain areas involved in depressive-like behavior by immunostaining. Interestingly, the PVT and medial prefrontal cortex (mPFC) were activated by DSS with a large number of c-fos-labeled neurons and protein expression

levels. The number of c-fos-labeled neurons did not differ in the hippocampal CA3, amygdala, and nucleus accumbens (Fig. 1E and F; in the PVT, Ctrl *vs* DSS, $P<0.0001$; in the mPFC, Ctrl *vs* DSS, $P<0.0001$). Some reports have demonstrated that depressive-like behaviors are associated with impairments of neuroplasticity in the mPFC [19]. The PVT plays a potential role in emotional behaviors. Moreover, in the present study, the number of c-fos positive cells in the PVT of DSS mice was much greater than that in the mPFC (Fig. 1E; in DSS, PVT *vs* mPFC $P<0.0001$).

RT-PCR showed that, in the PVT, DSS increased the IL-6 and IL-1β mRNA levels (Fig. 1G; in IL-6, Ctrl *vs* DSS, $P<0.0001$; in IL-1β, Ctrl *vs* DSS, $P<0.0001$). The microglial phenotype was characterized by immunostaining for Iba-1 (Fig. 1H). Microglial morphology suggested DSS-induced microglial activation in the PVT with a reduction of microglial branches (Fig. 1I; Ctrl *vs* DSS, $P<0.0001$), although no significant difference was found in maximum branch length (Fig. 1L; Ctrl *vs* DSS, $P=0.3615$). The Golgi staining demonstrated that the number of dendritic spines in the PVT of DSS mice was much less than that in Ctrl mice (Fig. 1J and K; Ctrl *vs* DSS, $P<0.0001$). The mice with DSS-induced colitis displayed increased levels of pro-inflammatory cytokines, microglial activation, and dendritic spine loss in the PVT, suggesting that the PVT plays an important role in DSS-induced depressive-like behaviors.

## Elevated Lcn2 in the PVT is Involved in DSS-induced Depressive Behaviors

The PVT has characteristic neural connections projecting to the posterior pituitary. It serves as a key node in modulating positive and negative behaviors [20]. To investigate the mRNA profile within the PVT in the normal and DSS mice, RNA-seq high-throughput sequencing was applied to determine the gene expression changes in DSS-induced depressive-like behaviors. The heatmaps showed 208 PVT genes that were significantly different between DSS and normal mice with a cutoff threshold of a fold change of 2.0 and $P<0.05$. 157 genes were upregulated and 51 were downregulated (Fig. 2A). Differentially-expressed mRNAs are displayed after fold change filtering, with statistically significant differential changes in mRNAs between the two groups identified with volcano plot filtering (Fig. 2B). The most enriched GO terms showed the numbers of differentially-expressed mRNAs were in biological process, cellular component, and molecular function (Fig. 2C). The DEGs from "membrane", "metal ion binding", and "immune system process" were involved in DSS-induced depressive-like behaviors. The KEGG analysis showed pathway enrichment for DSS mice and normal mice in the PVT. A previous report indicated a significantly higher concentration of the proinflammatory cytokine TNF-alpha in depressed patients compared with controls [21]. The result of the TNF signal pathway in previous research corresponded with the KEGG analysis in the current study (Fig. 2D).

To find critical genes in the PVT, the 20 top DEGs from the RNA-seq were identified by RT-PCR. The analysis showed that Lcn2 ($P<0.0001$), Lrg1 ($P<0.0001$), APod1 ($P<0.0001$), Acer2 ($P=0.0324$), S100a8 ($P=0.0239$), and Mt1 ($P=0.0321$) were increased in the PVT of DSS mice compared with control mice (Fig. 3A). The protein levels of Lcn2, Apod1, and Lrg1 were measured by western blotting (Fig. 3B). The semi-quantitative analysis suggested that the expression of Lcn2 was increased significantly in the PVT of DSS mice compared with controls (Fig. 3C; $P=0.0164$). The expression of Apod1 and Lrg1 did not statistically differ between DSS and Ctrl mice. The immunostaining results for Lcn2 corresponded with the western blotting analysis (Fig. 3D and E; $P<0.001$). The above results suggested that Lcn2 in the PVT plays an important role in DSS-induced depressive behaviors.

## Lcn2 shRNA Relieves DSS-Induced Pro-inflammatory Cytokines

To test the effect of Lcn2 in DSS mice, CMV-Lcn2 shRNA adeno-associated virus and the scrambled virus were injected into the PVT. Two weeks later, the mice were given 2.5% DSS for 5 days, followed by drinking water for 2 days. This procedure was repeated for one more cycle. The injection sites were validated at the end of the experiment (Fig. 4A) and the PVT was harvested for western blotting and RT-PCR. The blots indicated that the expression of Lcn2 was higher in DSS mice than in Ctrl mice. Lcn2 shRNA decreased the high level of Lcn2 induced by DSS (Fig. 4; BD Ctrl+scrambled *vs* DSS+scrambled $P<0.001$; Ctrl+scrambled *vs* Ctrl+Lcn2 shRNA $P=0.0018$; DSS+scrambled *vs* DSS+Lcn2shRNA $P<0.001$). In the PCR results, Lcn2 shRNA relieved the increasing level of IL-6 and IL-1β in the PVT after DSS treatment (Fig. 4C; IL-6: scrambled *vs* DSS+scrambled $P<0.001$; DSS+scrambled *vs* DSS+Lcn2shRNA $P=0.0232$; IL-1β: scrambled *vs* DSS+scrambled $P<0.001$; DSS+scrambled *vs* DSS+Lcn2shRNA $P=0.0375$).

## Lcn2 shRNA Alleviates the Dendritic Spine Loss Induced by DSS

To investigate the subtype of cells in which Lcn2 was expressed in the PVT, we used immunostaining with Lcn2 and NeuN (a neuronal marker), GFAP (an astrocytic marker), or iba1 (a microglial marker) in the PVT. The

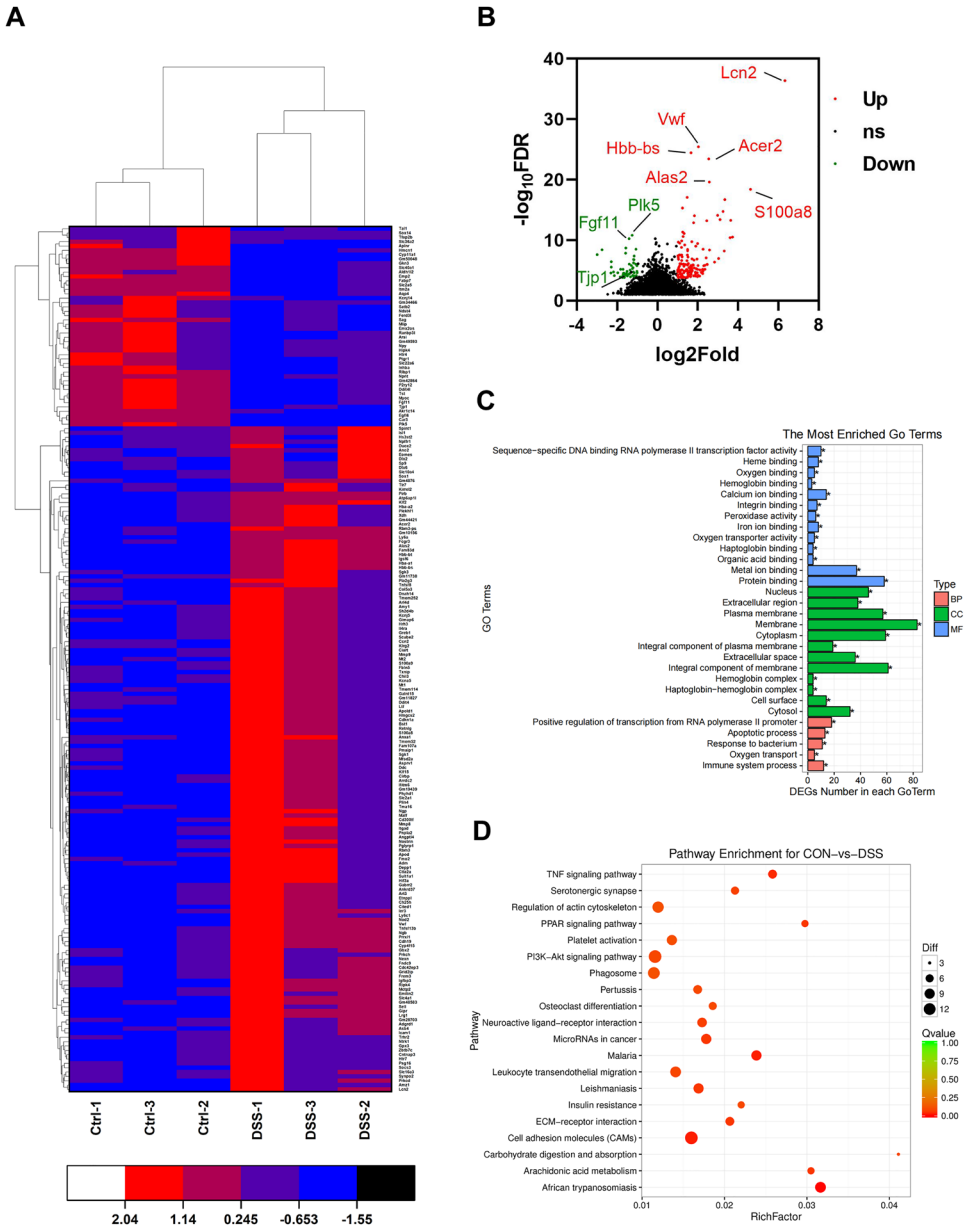


**Fig. 2** RNA-sequencing in the PVT of control mice and DSS mice. **A** Hierarchical clustering from 208 DEGs in the PVT between control mice and DSS mice. **B** Volcano plots show the distribution of DEGs. **C** GO terms analysis of DEGs. **D** KEGG pathway analysis of DEGs; size of dots corresponds to adjusted *P* values.

results showed that Lcn2 was colocalized with NeuN, and not with GFAP or iba1 (Figs 5A and S1) To verify the effect of Lcn2 on dendritic spines, we counted the number of dendritic spines by Golgi staining in the PVT after DSS and Lcn2 shRNA treatment. The results showed that DSS decreased the number of dendritic spines in the PVT of mice injected with the vehicle virus (Fig. 5B and C; scrambled *vs* DSS+scrambled $P < 0.0001$). However, Lcn2 shRNA rescued the reduced number of dendritic spines induced by DSS (Fig. 5B and C; DSS+scrambled *vs* DSS+Lcn2 shRNA $P = 0.0032$). These results indicated that Lcn2 is expressed on neurons and Lcn2 shRNA alleviates the dendritic spine loss induced by DSS.

## Upregulated Lcn2 Mediates Microglial Activation

What is the effect of Lcn2 on microglial activation in the PVT after DSS treatment? As a secreted protein, Lcn2 plays an important role as a chemokine inducer under inflammatory conditions of the CNS [22]. In our current study, SH-SY5Y cells were incubated with recombinant Lcn2 protein (1 or 10 μg/mL) for 6, 12, or 24 h, and total RNA was isolated for real-time RT-PCR. The mRNA levels of CCL2, CX3CL1, IL-1β, and IL-6 were determined. The mRNA levels of CCL2, CX3CL1, and IL-1β were dose- and time-dependently increased by Lcn2 protein, and the mRNA level of IL-6 was upregulated by Lcn2

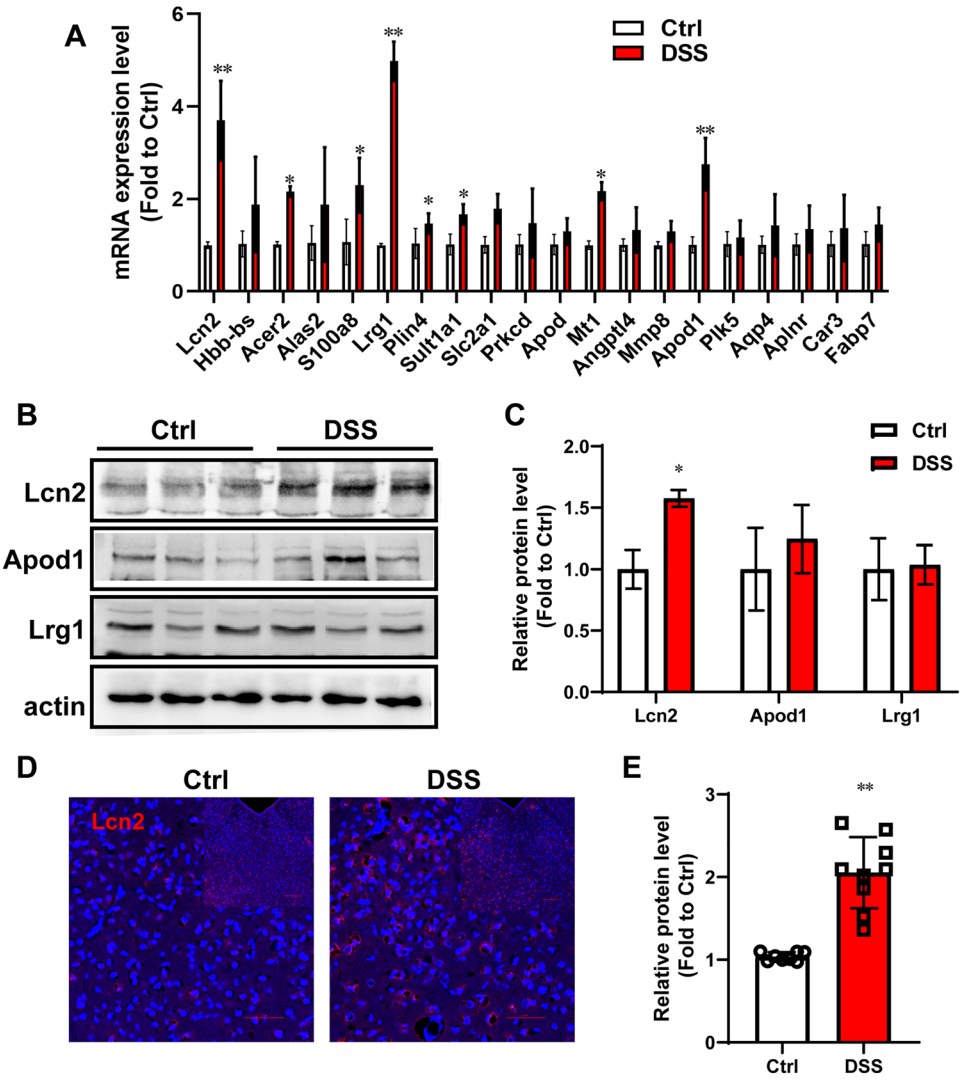


**Fig. 3** Lcn2 is upregulated in the PVT after DSS treatment. **A** RT-PCR for the 20 top DEGs from RNA-sequencing ($n=6$). **B** Amounts of Lcn2, Apod1, and Lrg1 in the PVT of control mice and DSS mice. **C** Semi-quantitative analyses of Lcn2, Apod1, and Lrg1 ($n=5$ mice/group). **D** Representative immunofluorescence staining of Lcn2 in the mice in the baseline and DSS groups. Scale bars, 50 μm, and 100 μm. **E** Semi-quantitative analysis of Lcn2 ($n=3$ mice/group). The data are presented as the mean ± SD. The two-tailed Student's *t*-test was used for **A** and **C**; the *t*-test was used for **E**. $^{*}P<0.05$. $^{**}P<0.01$.

protein at 24 h. These results suggested that, as a protein secreted by neurons, Lcn2 induced the expression of chemokines (CCL2 and CX3CL1) and cytokines (IL-1β and IL-6). Some studies have reported that elevated levels of chemokines and cytokines induce microglial activation [23–25]. To determine the influence of Lcn2 on microglial activation, we applied immunostaining for Iba-1. The representative images of Iba-1 indicated the microglia phenotype (Fig. 6E). Analysis of microglial morphology suggested that Lcn2 shRNA increased the number of microglial branches after DSS administration (Fig. 5F; DSS+scrambled *vs* DSS+Lcn2 shRNA $P<0.001$). Lcn2 shRNA did not affect the maximum branch length of microglia (Fig. 5G) Lcn2 silencing relieved the activation of microglia induced by DSS. Upregulated Lcn2 in the neurons of the PVT mediated microglial activation.

## Lcn2 is Required for DSS-Induced Depressive Behaviors

In the depressive behavior tests, Lcn2 shRNA did not influence the overall distance in the open-field test with DSS administration (Fig. 7A). In the forced swimming test, there were no statistical differences in immobile duration between scrambled+DSS mice and Lcn2 shRNA+DSS mice (Fig. 7B; scrambled+DSS *vs* Lcn2 shRNA+DSS $P=0.1430$). Lcn2 silencing rescued the immobile duration in the tail suspension test induced by DSS (Fig. 7C; scrambled+DSS *vs* Lcn2 shRNA+DSS $P=0.0078$) and elevated the preference percentage in the sucrose preference test (Fig. 7D; scrambled+DSS *vs* Lcn2 shRNA+DSS $P=0.0003$). Lcn2 shRNA alleviated the DSS-induced depressive behaviors. The biochemical tests and behavior tests suggested that Lcn2 is required for DSS-induced depressive behaviors.

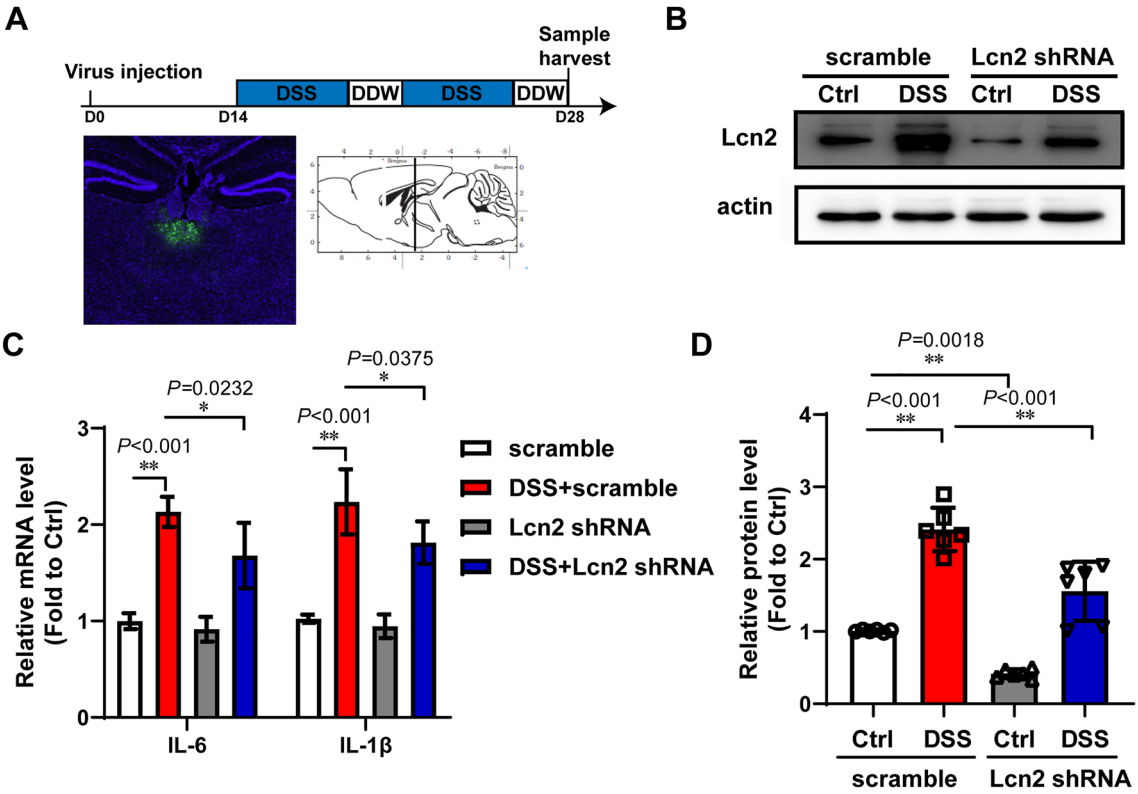


**Fig. 4** Lcn2 reduces the inflammatory cytokines in the PVT of DSS mice. **A** Experimental design. The wild-type mice at 6 weeks were injected with Lcn2 shRNA recombinant adeno-associated virus into the PVT, then after 2 weeks the mice were given 2.5% DSS in the drinking water for 2 cycles lasting 2 weeks. The injection sites were post-validated at the end of the experiment. **B** Amounts of Lcn2 in the PVT of control mice and DSS mice with Lcn2 shRNA virus or scrambled virus. **C** The mRNA levels of IL-6 and IL-1β in the PVT of DSS mice and normal mice with Lcn2 shRNA virus or scrambled virus ($n=8$). **D** Semi-quantitative analyses of Lcn2 ($n=6$). The data are presented as the mean ± SD. $^{*}P<0.05$. $^{**}P<0.01$. Two-way ANOVA was used for **C** and **D**).

### Lcn2 Mediates the Permeability of the Blood-Brain Barrier

From the RNA-seq analysis, the "TNF signaling pathway" and "cell adhesion molecules" were regulated in the PVT, and Tight junction protein 1 (TJP1, also known as ZO-1), which affects the integrity of the BBB [26], was downregulated in DSS mice. Previous research suggested that Lcn2 deficiency decreases proinflammatory cytokines and adhesion molecules (ICAM-1) [27], which could influence BBB permeability. Moreover, elevated Lcn2 levels are a likely cause for the induction of BBB dysfunction [28]. We determined whether Lcn2 affects BBB breakdown in the PVT after DSS treatment. In the western blotting assay, the expression levels of ZO-1 and Claudin5 were reduced in the DSS mice compared with control mice (Fig. 8A and B; ZO-1: $P<0.001$; Claudin5: $P<0.001$). Furthermore, Lcn2 shRNA rescued the expression level of ZO-1 and Claudin5 in the DSS mice (Fig. 8C and D; ZO-1: scrambled+DSS *vs* Lcn2 shRNA+DSS $P=0.0225$; Claudin5 scrambled+DSS *vs* Lcn2 shRNA+DSS $P=0.0002$). Wnt signaling has been reported to be a master regulator of BBB repair [29]. In the current study, we found that the expression of β-Catenin, the critical component of canonical Wnt signaling, was also reduced in DSS mice. Lcn2 returned the expression of β-Catenin to normal (Fig. 8C and D; scrambled+Ctrl *vs* scrambled+DSS $P<0.001$; scrambled+DSS *vs* Lcn2 shRNA+DSS $P=0.0011$). We used Evans blue to measure the BBB permeability. The results of Evans blue staining cannot be observed directly (Supplementary Fig. S4A). After the brain was imaged, the PVT was harvested from all mice. The quantitative measurement of EB-albumin extravasation was determined using a microplate reader at a wavelength of 610 nm. The results revealed that BBB permeability increased after DSS treatment, and Lcn2 shRNA rescued the EB extravasation (Supplementary Fig. S4B; scrambled+Ctrl *vs* scrambled+DSS $P=0.0046$; scrambled+DSS *vs* Lcn2 shRNA+DSS $P=0.0118$). In the extravascular IgG staining assay, DSS increased the extravascular IgG. The level of extravascular IgG was lower in the DSS+Lcn2 shRNA group than in the DSS+scrambled group (Supplementary Fig. S4C and D; scrambled+Ctrl *vs* scrambled+DSS $P<0.001$;

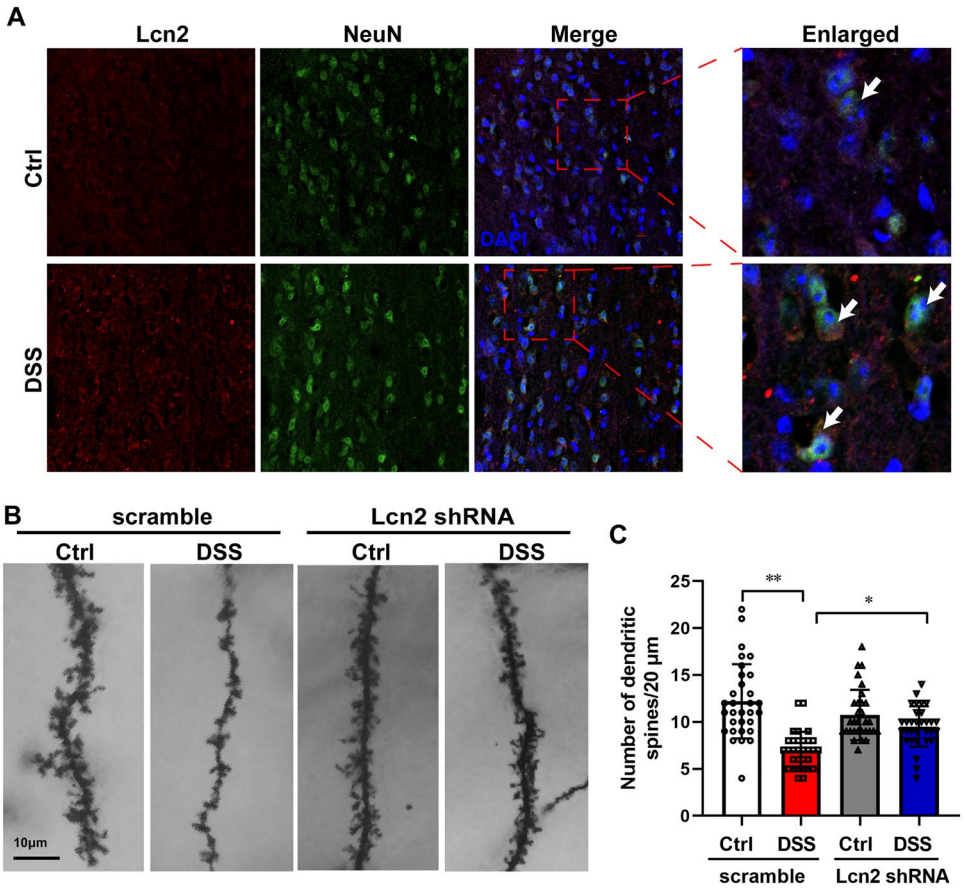


**Fig. 5** Lcn2 is expressed on neurons and the Lcn2 shRNA virus improved dendritic spines after DSS treatment. **A** Representative immunofluorescence staining of Lcn2 and NeuN in the PVT of mice in the baseline and DSS groups ($n=6$). **B** Representative images of Golgi staining in the paraventricular thalamic nucleus of mice after DSS treatment and Lcn2 shRNA virus injection. **C** Analysis of the number of dendritic spines at the unit of 20 μm ($n=6$). More than 30 images were counted for each group. The data were presented as means ± SD. Two-way ANOVA was used for **C**. $^{*}P<0.05$. $^{**}P<0.01$.

scrambled+DSS *vs* Lcn2 shRNA+DSS $P<0.001$). In the immunostaining assay, the tendency of the expression of ZO-1 and Lcn2 was in accordance with the results from the western blotting assays (Fig. 8E and F; Lcn2: scrambled *vs* scrambled+DSS $P<0.001$; scrambled+DSS *vs* Lcn2 shRNA+DSS $P=0.0003$; ZO-1: scrambled *vs* scrambled+DSS $P=0.0197$; scrambled+DSS *vs* Lcn2 shRNA+DSS $P=0.0205$). And Lcn2 was co-localized with the tight junction-specific protein ZO-1, suggesting that Lcn2 mediates BBB permeability through the interaction between Lcn2 and ZO-1 in the PVT after DSS treatment.

## Discussion

Evidence has shown that the incidence of psychiatric disorders in IBD patients is higher than in the general population [1, 30, 31]. Repeated administration of DSS in drinking water is regarded as a well-characterized mouse model of IBD [32, 33]. A couple of studies reported that DSS mice exhibit depressive-like behavior [34, 35]. However, the underlying mechanism of DSS-induced depressive-like behavior was still unclear. In our work, we identified that the PVT was activated after repeated DSS administration. RNA high-throughput sequencing was used to explore the effect of PVT on depressive-like behavior in DSS mice. We found that upregulated Lcn2 in the PVT was required for depressive behavior after DSS treatment. Upregulating Lcn2 from neuronal activity induced dendritic spine loss and the secreted protein induced chemokine expression and subsequent microglial activation leading to BBB permeability. These data for the first time demonstrated that Lcn2 in the PVT is critical for the depressive-like behavior induced by DSS.

Several studies have identified the critical role of hippocampal neurogenesis in linking depressive-like behaviors in DSS-treated mice with the increased levels of inflammatory cytokines and activation of microglia and astrocytes in the hippocampus [18, 36]. However, alteration of inflammatory markers induced by DSS treatment changes depending on the brain region [7], indicating that region-specific expression level change of markers may support the underlying mechanisms of depressive-like behavior in DSS mice. Therefore, we used c-Fos as a proxy of neural activity and the PVT and mPFC showed a significantly higher proportion of c-Fos signals than controls. In the current study, the number of c-fos-positive cells in the PVT of DSS mice was much greater than that in control mice, supporting a potential role of the PVT in DSS-induced depressive behaviors (Fig. 1E, F). Placed in the dorsal midline thalamus, the PVT is involved in the

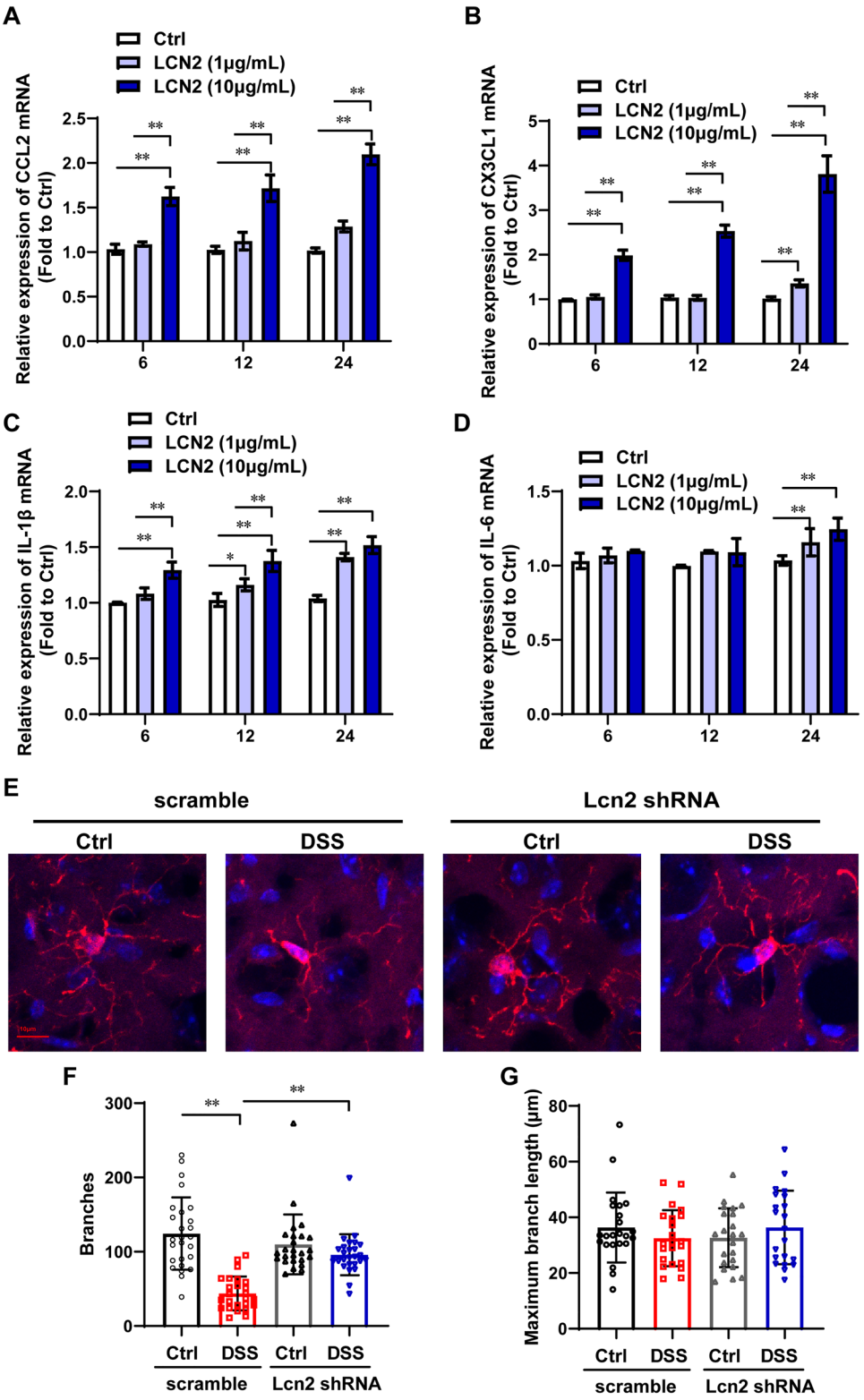


**Fig. 6** Lcn2 induces the chemokine gene expression and Lcn2 shRNA virus revised microglial activation. **A–D** SH-SY5Y cells were incubated with recombinant Lcn2 protein (1 or 10 μg/mL) for 6, 12, or 24 h, and total RNA was isolated for real-time RT-PCR. The mRNA levels of CCL2 (**A**), CX3CL1 (**B**), IL-1β (**C**), and IL-6 (**D**) were determined. All samples were triple holes. This experiment had been repeated three times. **E** Representative images of the expression of Iba-1 in the paraventricular thalamic nucleus of mice after DSS treatment and Lcn2 shRNA virus injection by immunostaining. **F–G** Microglial morphology was analyzed ($n=6$) More than 30 images were analyzed for each group. The data were presented as means ± SD. Two-way ANOVA was used for **A, B, C, D, F,** and **G**. $^{*}P<0.05$. $^{**}P<0.01$.

regulation of stress and functions in several psychiatric disorders including anxiety and major depressive disorders [20]. After the forced swimming test, the PVT with increasing levels of c-Fos was associated with the levels of immobility, [37] and PVT neurons projecting to the CeA regulate depressive-like behaviors in a sex-dependent manner [38]. In our study, the PVT and mPFC were activated in DSS mice according to c-fos-labeled neurons

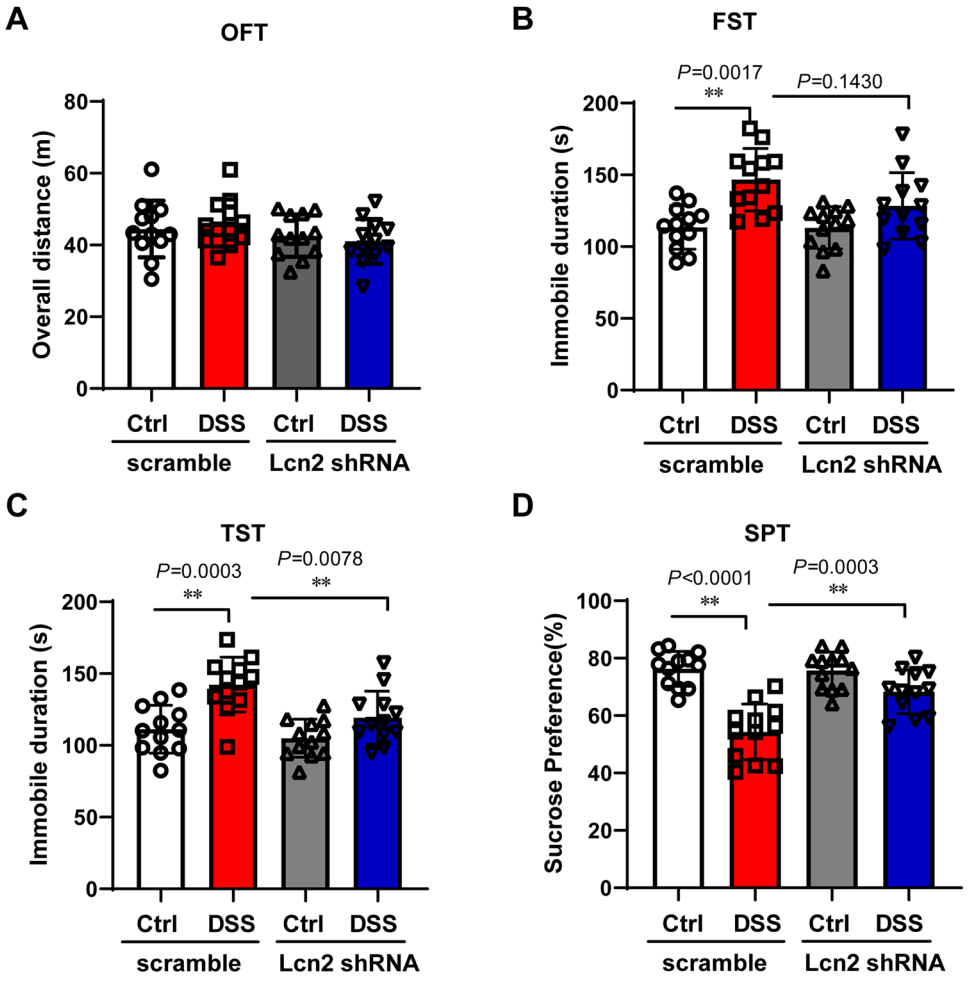


**Fig. 7** Lcn2 shRNA rescues the DSS-induced depressive-like behaviors. The wild-type mice were injected with Lcn2 shRNA recombinant adeno-associated virus into PVT, then after 2 weeks the mice were administrated with 2.5% DSS lasting 2 weeks. At the end of DSS cycles, behavior tests were measured. **A** Open filed ($n=12$), **B** forced swimming test ($n=12$), **C** tail suspension test ($n=12$), and **D** sucrose preference test ($n=12$) were shown. The data were presented as means ± SD. Two-way ANOVA was used for **A, B, C,** and **D**. $^{*}P<0.05$. $^{**}P<0.01$.

(Fig. 1E, F). We hypothesize that the mPFC-PVT circuit may be involved in DSS-induced depressive behaviors. The neurons in the PVT were activated by the elevated Lcn2 in a short time after DSS treatment, and the mPFC may receive projections from the PVT mediating the DSS-induced depressive behaviors. Lcn2 is well described to participate in the innate immune response and regulate neuronal excitability. Lcn2-null mice have been reported to exhibit synaptic impairment in long-term potentiation in the hippocampus resulting in stress-induced anxiety [39]. However, another study argued that a high level of expression of Lcn2 occurs with the depression-like behavior of LPS-treated mice [40]. In our work, the upregulation of Lcn2 was assessed in the RNA-sequencing analysis, and its sufficient role in the PVT of DSS mice was determined by RT-PCR and western blot assays (Figs. 2 and 3). The discrepancy of Lcn2 in emotional behavior may be attributed to the brain region-specific expression of Lcn2. Both the WT and lcn2$^{-/-}$ mice after LPS treatment presented equivalent reductions in sucrose preference and TST immobility [40]. However, in our study, Lcn2 silencing in the PVT alleviated the depressive-like behaviors in DSS mice (Fig. 7), suggesting that a high level of Lcn2 in the PVT is required for the depressive symptoms.

The results of immunostaining showed that Lcn2 and its receptor 24p3R were co-localized with neurons (Fig. 5A and Supplementary Figs S1 and S3). Previous studies have suggested that dendritic cell factor 1 triggers the dendritic spine and synaptic function by regulating the expression of Lcn2 [41, 42]. In our study, Lcn2 shRNA rescued the reduction in the number of dendritic spines induced by DSS (Fig. 5B, C). Lcn2 was expressed on neurons, which partly explained the morphological change in dendritic spines after DSS treatment. As a secreted protein, Lcn2 plays an important role as a chemokine inducer under inflammatory conditions of the CNS [22, 43]. In our study, upregulation of the TNF signaling pathway from the KEGG Enrichment pathway analysis (Fig. 2D) and increasing levels of IL-6 and IL-1β from the RT-PCR results (Fig. 1G) suggested the relationship between upregulation of cytokines and the increasing level of Lcn2 in the PVT after DSS treatment. In the current study, recombinant Lcn2 protein induced the expression of chemokines (CCL2 and CX3CL1) and cytokines (IL-1β and IL-6) in SH-SY5Y cells (Fig. 6A-D). High levels of chemokines and cytokines induce microglial activation [23–25], and Lcn2 shRNA increased the number of microglial branches after

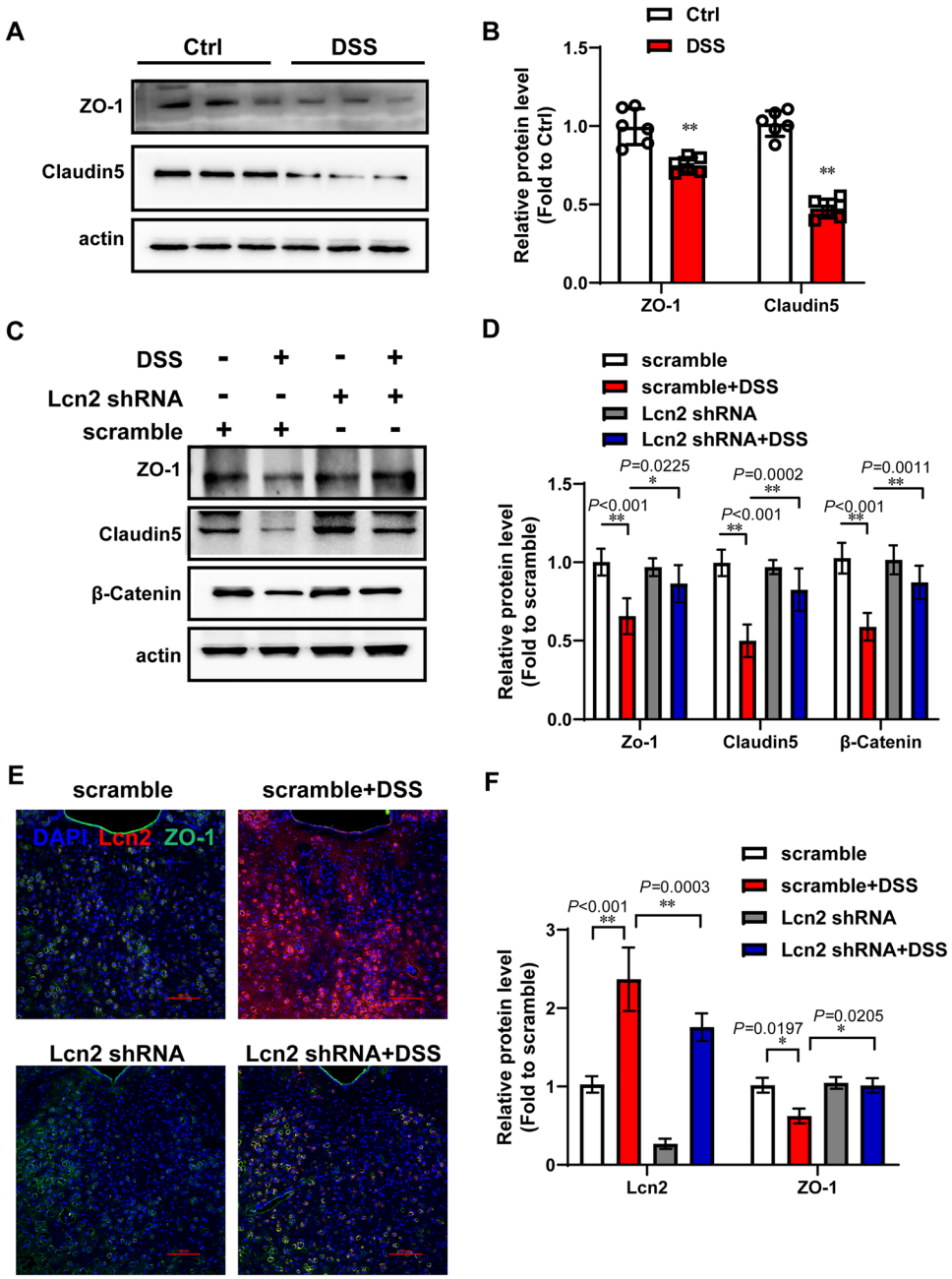


**Fig. 8** Lcn2 might mediate BBB permeability. **A** Amounts of ZO-1 and Claudin5 in the PVT of control mice and DSS mice. **B** Semi-quantitative analyses of ZO-1 and Claudin5 ($n=6$ mice/group). **C** Amounts of ZO-1, Claudin5, and β-Catenin in the PVT of mice after DSS treatment and Lcn2 shRNA injection. **D** Semi-quantitative analyses of ZO-1, Claudin5, and β-Catenin ($n=6$ mice/group). **E** Representative images of the expression of Lcn2 and ZO-1 in the paraventricular thalamic nucleus of mice after DSS treatment and Lcn2 shRNA injection. Scale bars, 100 μm. **F** Semi-quantitative analysis of Lcn2 and ZO-1 ($n=5$ mice/group). The data are presented as the mean ± SD. Two-way ANOVA was used for **B**, **D**, and **F**. $^{*}P<0.05$. $^{**}P<0.01$.

DSS administration (Fig. 6E-G). Above all, in the PVT of mice after DSS treatment, neuron-derived Lcn2 induced chemokine expression and subsequently contributed to microglial activation. However, one study has reported that Lcn2 plays an important role in regulating mood disorders, controls hippocampal neurogenesis in adults, and regulates hippocampal microglial activation in poststroke depression [44]. This does not allow us to conclude that DSS-induced depressive behavior is driven exclusively by Lcn2 in the PVT. More experiments are needed.

Previous studies have reported that Lcn2 protein and mRNA expression are upregulated in the colon mucosa of active collagenous colitis patients [45] and serum Lcn2 is significantly upregulated in patients with active IBD [46]. In our study, we used immunohistochemistry to measure the Lcn2 expression in the colon of DSS mice and found that it was upregulated (Supplementary Fig. S2A, B). The results suggested that the elevated Lcn2 in the PVT of the DSS model came from the colon mucosa *via* circulation. Neuron-derived Lcn2 induces chemokine expression and subsequently contributes to microglial activation. Microglia play an important role in maintaining BBB integrity. Vessel-associated microglia initially maintain BBB integrity *via* the expression of the tight-junction protein

Claudin-5 [47]. In our study, microglial activation may induce BBB permeability after DSS treatment (Fig. 8A, B). Lcn2 shRNA rescued the expression level of ZO-1 and Claudin5 in the DSS mice (Fig. 8C, D) and Lcn2 silencing alleviated the BBB permeability according to the analysis of Evans blue staining and IgG staining (Supplementary Fig. S4). Moreover, Lcn2 was co-localized with the ZO-1 (Fig. 8E, F). Microglial activation may promote BBB permeability through the interaction between Lcn2 and ZO-1. Above all, upregulating Lcn2 from neuronal activity after DSS treatment induced dendritic spine loss, and the secreted protein induced chemokine expression and subsequent microglial activation leading to BBB permeability.

In clinical practice, there are no effective biochemical indicators for evaluating depressive-like behaviors in IBD patients. The level of Lcn2 can be measured in plasma [51] and urine [52] in clinical applications. Our study provides a potential strategy to predict the risk of depressive disorder induced by IBD in plasma or urine.

Our RNA-sequencing analysis suggested a relationship between T cell activation and depressive symptoms in DSS mice. The RNA-sequencing results indicated an increasing level of S100A8 in the PVT of DSS mice (Fig. 2B). One report has suggested the upregulation of S100A8 may be involved in the morphological change in microglia induced by the infiltration of peripheral inflammatory cells into the brain [53]. More essential evidence is needed to demonstrate the potential role of S100A8 in the depressive-like behaviors induced by DSS treatment.

Taken together, in the current study we explored the underlying mechanism of DSS-induced depression-like behaviors. We showed that PVT plays an important role in the depressive symptoms of DSS mice. Upregulating Lcn2 from neuronal activity in the PVT after DSS treatment induced dendritic spine loss and the secreted protein-induced chemokine expression caused subsequent microglial activation leading to BBB permeability. We have shown conclusively for the first time that elevated Lcn2 in the PVT contributes to DSS-induced depression-like behaviors. The present study provides a novel therapeutic target in DSS-induced depressive-like behaviors.

**Acknowledgments** We are grateful for the technical support of the Core Facilities, Zhejiang University School of Medicine. This work was supported by the National Natural Science Foundation of China (82001424 and 82171176), and the Key Program of the Natural Science Foundation of Zhejiang, China (LZ19H090003).

## References

1. Barberio B, Zamani M, Black CJ, Savarino EV, Ford AC. Prevalence of symptoms of anxiety and depression in patients with inflammatory bowel disease: A systematic review and meta-analysis. Lancet Gastroenterol Hepatol 2021, 6: 359–370.
2. Jordi SBU, Lang BM, Auschra B, von Känel R, Biedermann L, Greuter T. Depressive symptoms predict clinical recurrence of inflammatory bowel disease. Inflamm Bowel Dis 2022, 28: 560–571.
3. Moulton CD, Pavlidis P, Norton C, Norton S, Pariante C, Hayee B, *et al*. Depressive symptoms in inflammatory bowel disease: An extraintestinal manifestation of inflammation? Clin Exp Immunol 2019, 197: 308–318.
4. Chen LM, Bao CH, Wu Y, Liang SH, Wang D, Wu LY, *et al*. Tryptophan-kynurenine metabolism: A link between the gut and brain for depression in inflammatory bowel disease. J Neuroinflammation 2021, 18: 135.
5. Sandes S, Figueiredo N, Pedroso S, Sant'Anna F, Acurcio L, Abatemarco Junior M, *et al*. *Weissella paramesenteroides* WpK4 plays an immunobiotic role in gut-brain axis, reducing gut permeability, anxiety-like and depressive-like behaviors in murine models of colitis and chronic stress. Food Res Int 2020, 137: 109741.
6. Natah SS, Mouihate A, Pittman QJ, Sharkey KA. Disruption of the blood-brain barrier during TNBS colitis. Neurogastroenterol Motil 2005, 17: 433–446.
7. Do J, Woo J. From gut to brain: Alteration in inflammation markers in the brain of dextran sodium sulfate-induced colitis model mice. Clin Psychopharmacol Neurosci 2018, 16: 422–433.
8. McGinty JF, Otis JM. Heterogeneity in the paraventricular thalamus: The traffic light of motivated behaviors. Front Behav Neurosci 2020, 14: 590528.
9. Barson JR, Mack NR, Gao WJ. The paraventricular nucleus of the thalamus is an important node in the emotional processing network. Front Behav Neurosci 2020, 14: 598469.
10. Jha MK, Lee S, Park DH, Kook H, Park KG, Lee IK, *et al*. Diverse functional roles of lipocalin-2 in the central nervous system. Neurosci Biobehav Rev 2015, 49: 135–156.
11. Olson B, Zhu X, Norgard MA, Diba P, Levasseur PR, Buenafe AC, *et al*. Chronic cerebral lipocalin 2 exposure elicits hippocampal neuronal dysfunction and cognitive impairment. Brain Behav Immun 2021, 97: 102–118.
12. Yang Y, Cui Y, Sang K, Dong Y, Ni Z, Ma S, *et al*. Ketamine blocks bursting in the lateral habenula to rapidly relieve depression. Nature 2018, 554: 317–322.
13. Peng Z, Li X, Li J, Dong Y, Gao Y, Liao Y, *et al*. Dlg1 knockout inhibits microglial activation and alleviates lipopolysaccharide-induced depression-like behavior in mice. Neurosci Bull 2021, 37: 1671–1682.
14. Zheng P, Zeng B, Zhou C, Liu M, Fang Z, Xu X, *et al*. Gut microbiome remodeling induces depressive-like behaviors through a pathway mediated by the host's metabolism. Mol Psychiatry 2016, 21: 786–796.
15. Chen Y, Zhang P, Lin X, Zhang H, Miao J, Zhou Y, *et al*. Mitophagy impairment is involved in sevoflurane-induced cognitive dysfunction in aged rats. Aging (Albany NY) 2020, 12: 17235–17256.
16. Xia M, Li Z, Li S, Liang S, Li X, Chen B, *et al*. Sleep deprivation selectively down-regulates astrocytic 5-$HT_{2B}$ receptors and triggers depressive-like behaviors via stimulating $P2X_7$ receptors in mice. Neurosci Bull 2020, 36: 1259–1270.
17. Chen YR, Zhang SX, Fang M, Zhang P, Zhou YF, Yu X, *et al*. Egr2 contributes to age-dependent vulnerability to sevoflurane-induced cognitive deficits in mice. Acta Pharmacol Sin 2022, 43: 2828–2840.
18. Bisgaard TH, Allin KH, Keefer L, Ananthakrishnan AN, Jess T. Depression and anxiety in inflammatory bowel disease: Epidemiology, mechanisms and treatment. Nat Rev Gastroenterol Hepatol 2022, 19: 717–726.
19. Price RB, Duman R. Neuroplasticity in cognitive and psychological mechanisms of depression: An integrative model. Mol Psychiatry 2020, 25: 530–543.
20. Hsu DT, Kirouac GJ, Zubieta JK, Bhatnagar S. Contributions of the paraventricular thalamic nucleus in the regulation of stress, motivation, and mood. Front Behav Neurosci 2014, 8: 73.

21. Das R, Emon MPZ, Shahriar M, Nahar Z, Islam SMA, Bhuiyan MA, *et al*. Higher levels of serum IL-1β and TNF-α are associated with an increased probability of major depressive disorder. Psychiatry Res 2021, 295: 113568.
22. Lee S, Kim JH, Kim JH, Seo JW, Han HS, Lee WH, *et al*. Lipocalin-2 Is a chemokine inducer in the central nervous system: Role of chemokine ligand 10 (CXCL10) in lipocalin-2-induced cell migration. J Biol Chem 2011, 286: 43855–43870.
23. Jeon S, Jha MK, Ock J, Seo J, Jin M, Cho H, *et al*. Role of lipocalin-2-chemokine axis in the development of neuropathic pain following peripheral nerve injury. J Biol Chem 2013, 288: 24116–24127.
24. Monif M, Reid CA, Powell KL, Drummond KJ, O'Brien TJ, Williams DA. Interleukin-1β has trophic effects in microglia and its release is mediated by P2X7R pore. J Neuroinflammation 2016, 13: 173.
25. Zhang L, Tan J, Jiang X, Qian W, Yang T, Sun X, *et al*. Neuron-derived CCL2 contributes to microglia activation and neurological decline in hepatic encephalopathy. Biol Res 2017, 50: 26.
26. Watson PM, Anderson JM, Vanltallie CM, Doctrow SR. The tight-junction-specific protein ZO-1 is a component of the human and rat blood-brain barriers. Neurosci Lett 1991, 129: 6–10.
27. Jin M, Kim JH, Jang E, Lee YM, Han HS, Woo DK, *et al*. Lipocalin-2 deficiency attenuates neuroinflammation and brain injury after transient middle cerebral artery occlusion in mice. J Cereb Blood Flow Metab 2014, 34: 1306–1314.
28. Mondal A, Bose D, Saha P, Sarkar S, Seth R, Kimono D, *et al*. Lipocalin 2 induces neuroinflammation and blood-brain barrier dysfunction through liver-brain axis in murine model of nonalcoholic steatohepatitis. J Neuroinflammation 2020, 17: 201.
29. Gastfriend BD, Nishihara H, Canfield SG, Foreman KL, Engelhardt B, Palecek SP, *et al*. Wnt signaling mediates acquisition of blood-brain barrier properties in naïve endothelium derived from human pluripotent stem cells. Elife 2021, 10: e70992.
30. Rozich JJ, Holmer A, Singh S. Effect of lifestyle factors on outcomes in patients with inflammatory bowel diseases. Am J Gastroenterol 2020, 115: 832–840.
31. Neuendorf R, Harding A, Stello N, Hanes D, Wahbeh H. Depression and anxiety in patients with Inflammatory Bowel Disease: A systematic review. J Psychosom Res 2016, 87: 70–80.
32. Bauer C, Duewell P, Mayer C, Lehr HA, Fitzgerald KA, Dauer M, *et al*. Colitis induced in mice with dextran sulfate sodium (DSS) is mediated by the NLRP3 inflammasome. Gut 2010, 59: 1192–1199.
33. Zhou G, Yu L, Fang L, Yang W, Yu T, Miao Y, *et al*. CD177$^{+}$ neutrophils as functionally activated neutrophils negatively regulate IBD. Gut 2018, 67: 1052–1063.
34. Ancona A, Petito C, Iavarone I, Petito V, Galasso L, Leonetti A, *et al*. The gut-brain axis in irritable bowel syndrome and inflammatory bowel disease. Dig Liver Dis 2021, 53: 298–305.
35. Li Y, Zhang H, Yang J, Zhan M, Hu X, Liu Y, *et al*. P2Y12 receptor as a new target for electroacupuncture relieving comorbidity of visceral pain and depression of inflammatory bowel disease. Chin Med 2021, 16: 139.
36. Nakagawasai O, Yamada K, Takahashi K, Odaira T, Sakuma W, Ishizawa D, *et al*. Liver hydrolysate prevents depressive-like behavior in an animal model of colitis: Involvement of hippocampal neurogenesis via the AMPK/BDNF pathway. Behav Brain Res 2020, 390: 112640.
37. Zhu L, Wu L, Yu B, Liu X. The participation of a neurocircuit from the paraventricular thalamus to amygdala in the depressive like behavior. Neurosci Lett 2011, 488: 81–86.
38. Zhao D, Liu C, Cui M, Liu J, Meng F, Lian H, *et al*. The paraventricular thalamus input to central amygdala controls depression-related behaviors. Exp Neurol 2021, 342: 113744.
39. Ferreira AC, Pinto V, Mesquita SD, Novais A, Sousa JC, Correia-Neves M, *et al*. Lipocalin-2 is involved in emotional behaviors and cognitive function. Front Cell Neurosci 2013, 7: 122.
40. Vichaya EG, Gross PS, Estrada DJ, Cole SW, Grossberg AJ, Evans SE, *et al*. Lipocalin-2 is dispensable in inflammation-induced sickness and depression-like behavior. Psychopharmacology 2019, 236: 2975–2982.
41. Liu Q, Feng R, Chen Y, Luo G, Yan H, Chen L, *et al*. Dcf1 triggers dendritic spine formation and facilitates memory acquisition. Mol Neurobiol 2018, 55: 763–775.
42. Zheng L, Liu Q, Wen T. Dendritic cell factor 1 deletion leads to developmental defects in mushroom-shaped dendritic spines. Neuroreport 2019, 30: 1008–1015.
43. Borkham-Kamphorst E, Drews F, Weiskirchen R. Induction of lipocalin-2 expression in acute and chronic experimental liver injury moderated by pro-inflammatory cytokines interleukin-1β through nuclear factor-κB activation. Liver Int 2011, 31: 656–665.
44. Wei L, Du Y, Xie Y, Yu X, Chen H, Qiu Y. Lipocalin-2 regulates hippocampal microglial activation in poststroke depression. Front Aging Neurosci 2021, 13: 798335.
45. Bakke I, Walaas GA, Bruland T, Røyset ES, van Beelen Granlund A, Escudero-Hernández C, *et al*. Mucosal and faecal neutrophil gelatinase-associated lipocalin as potential biomarkers for collagenous colitis. J Gastroenterol 2021, 56: 914–927.
46. Stallhofer J, Friedrich M, Konrad-Zerna A, Wetzke M, Lohse P, Glas J, *et al*. Lipocalin-2 is a disease activity marker in inflammatory bowel disease regulated by IL-17A, IL-22, and TNF-α and modulated by IL23R genotype status. Inflamm Bowel Dis 2015, 21: 2327–2340.
47. Haruwaka K, Ikegami A, Tachibana Y, Ohno N, Konishi H, Hashimoto A, *et al*. Dual microglia effects on blood brain barrier permeability induced by systemic inflammation. Nat Commun 2019, 10: 5816.
48. Harry GJ. Microglia during development and aging. Pharmacol Ther 2013, 139: 313–326.
49. Vojdani A, Vojdani E, Herbert M, Kharrazian D. Correlation between antibodies to bacterial lipopolysaccharides and barrier proteins in sera positive for *ASCA* and ANCA. Int J Mol Sci 2020, 21: 1381.
50. Toyota Y, Wei J, Xi G, Keep RF, Hua Y. White matter T2 hyperintensities and blood-brain barrier disruption in the hyperacute stage of subarachnoid hemorrhage in male mice: The role of lipocalin-2. CNS Neurosci Ther 2019, 25: 1207–1214.
51. Oberoi R, Bogalle EP, Matthes LA, Schuett H, Koch AK, Grote K, *et al*. Lipocalin (LCN) 2 mediates pro-atherosclerotic processes and is elevated in patients with coronary artery disease. PLoS One 2015, 10: e0137924.
52. Guo P, Yang J, Jia D, Moses MA, Auguste DT. ICAM-1-targeted, Lcn2 siRNA-encapsulating liposomes are potent anti-angiogenic agents for triple negative breast cancer. Theranostics 2016, 6: 1–13.
53. Talley S, Valiauga R, Anderson L, Cannon AR, Choudhry MA, Campbell EM. DSS-induced inflammation in the colon drives a proinflammatory signature in the brain that is ameliorated by prophylactic treatment with the S100A9 inhibitor paquinimod. J Neuroinflammation 2021, 18: 263.